

An S-shaped Arc in the Galaxy Cluster RX J0054.0-2823[★]

C. Faure^{1,4}, E. Giraud², J. Melnick³, H. Quintana⁴, F. Selman³, and J. Wambsganss¹

¹ Zentrum für Astronomie der Universität Heidelberg (ZAH), Mönchhofstr. 12-14, 69120 Heidelberg, Germany

² Laboratoire Physique Théorique et Astroparticules, UMR5207 In2p3/Montpellier University, F-34095 Montpellier

³ European Southern Observatory, Alonso de Córdova 3107, Santiago, Chile

⁴ Department of Astronomy and Astrophysics, P. Universidad Católica de Chile, Casilla 306, Santiago, Chile

accepted 29/09/2006

Abstract. The center of the galaxy cluster RX J0054.0-2823 at $z = 0.292$ is a dynamically active region which includes an interacting system of three galaxies surrounded by a large halo of intra-cluster light. We report here the discovery of an S-shaped feature of total length $11''$ in the central region of this cluster and discuss its physical nature. We test the gravitational lensing assumption by doing a mass modelling of the central part of the galaxy cluster. We very naturally reproduce position and form of this S-shape feature as a gravitationally lensed background object at redshift between 0.5 and 1.0. We conclude that the lensing nature is the very probable explanation for this S-shaped arc; the ultimate proof will be the spectroscopic confirmation by measuring the high redshift of this elongated feature with surface brightness $V \sim 24$ mag arcsec⁻².

1. Introduction

Giant luminous arcs were discovered in 1986/87 (Lynds & Petrosian 1986, Soucail et al. 1987) and found to be highly distorted background galaxies, magnified and often multiply imaged by the gravitational lensing action of an intervening galaxy cluster (Paczynski 1987). Meanwhile, more than 100 giant arcs systems have been found (Gladders, Yee & Ellingson 2002 and references therein) and studied both to infer the cluster mass distribution and – using the magnification effect – to investigate the high redshift galaxy population (e.g., Colley, Tyson & Turner 1996). The ensemble of arcs was also used for statistical inferences regarding consistency with various cosmological models (e.g., Bartelmann et al. 1998; Golse, Kneib & Soucail 2002; Soucail, Kneib & Golse 2004; Wambsganss, Bode & Ostriker 2004; Sand et al. 2005).

Contrary to the implication of the name, the shapes of highly distorted background galaxies are not always curved like an arc: lots of radial arcs have been found, elongated features extended in the radial direction; a straight arc was discovered early on as well (Wambsganss et al. 1989). Here we report the discovery of a strangely shaped arc candidate. Our modelling shows that a very natural explanation for this S-shaped feature is a background galaxy gravitationally lensed by the moderately massive X-ray cluster RX J0054.0-2823, with the shape particularly affected by the three prominent central galaxies, and the cluster ellipticity.

2. Observations and data reduction

The galaxy cluster RX J0054.0-2823 was identified as part of the 160 square degree ROSAT serendipity survey (Vikhlinin et al. 1998, Mullis et al. 2003). Our imaging observations of RX J0054.0-2823 consist of a series of 24 V-band and 39 I-band images, with an exposure time of 300 s each, acquired during two photometric dark nights on 2000 September 26 and 27, using SUSI2 at the ESO NTT. The total exposure time was 18900s. SUSI2 covers a field of $5' \times 5'$ with two CCDs at a pixel scale of $0.0805''\text{pixel}^{-1}$. The CCDs were binned 2×2 . In order to correct for fringing, sky background and CCD variations, the observations were carried out with an alternating dithering pattern as described in Melnick, Selman & Quintana (1999). In this method, the cluster center is placed on one of the CCDs, say CCD1, while CCD2 simultaneously measures the sky background. Then the cluster is centered on CCD2, and CCD1 is used to measure the sky. The exposure is thus divided in a large number of integrations, nodding consecutively on CCD1 and CCD2, and off-setting the telescope by small random amounts to dither the images. The differences between consecutive images allow to correct for fringing, to built and subtract for darks and to remove for most systematic effects. The frames are flat-fielded by using a master flat. The final images, which are the medians of individual 300s exposures, are calibrated using Landolt stars (1992). A maximum variation by a factor of 2 was found in the I-band sky background over the two nights, with 3 main groups of values at 19.2, 19.5 and 19.9 mag arcsec⁻². The background noise depends on the number of individual images at a given position: in the central overlap area the 1σ isophotes are at $V = 27.0$ and $I = 25.7$ mag arcsec⁻² respectively. The connection between

[★] Based on observations obtained at the European Southern Observatory, La Silla, Chile and ESO archive files

pixels of real objects allows clear detections at these magnitudes. The full field size of our final image is $9.5' \times 5.5'$.

The galaxy spectra of RX J0054.0-2823 which we retrieved from the ESO archives (program 64.O-0455(A); P.I. H. Quintana) were originally obtained using EFOSC in multi-object spectroscopic mode (MOS) at the ESO 3.6m telescope. Two consecutive MOS spectra of the same galaxies with 1800s exposure time each, had been acquired during the night 1999 November 8 with atmospheric seeing of $0.9''$ and $0.8''$, respectively. They had been obtained with slitlets of $1.5''$ and Grism #6 which provides a wavelength coverage of 380-850 nm at a resolution of 2 nm ($R \sim 300$). The detector was binned 2×2 at readout giving a spectral dispersion of $0.4 \text{ nm pixel}^{-1}$ and a spatial scale of $0.31'' \text{ pixel}^{-1}$. The data were analyzed using the context LONG within MIDAS. The two-dimensional spectra were corrected for bias and flat-field and wavelength calibrated using HeAr lines. One-dimensional spectra were then extracted after sky subtraction. Redshifts were measured by fitting the continuum and the identified lines by using the MIDAS context ALICE. They are based on [OII], the CaII H and K doublet, the Mgb band, NaID, and the Balmer lines. Eighteen individual galaxy redshifts were thus obtained (all indicated in Fig. 1) out of which 14 turned out to be cluster members (see also redshift histogram in Fig. 3).

3. The galaxy cluster: images and redshifts

The V-band image of galaxy cluster RX J0054.0-2823 is shown in Fig. 1. On a $4'$ ($1.3 h_{75}^{-1} \text{ Mpc}$) scale, the main feature is an apparently elongated distribution of galaxy traced by a few bright galaxies at $\text{PA} \sim 30^\circ$ with a concentration around 3 major objects in close contact, surrounded by a common envelope, which is also the location of the X-ray emission detected by ROSAT (Mullis et al. 2003). The central galaxy triplet (see top right insert of Fig. 1) is made of a close pair of elliptical galaxies (labeled #131 and #139 in Fig. 4), and a more elongated object (#128). On a scale of $25''$ ($\sim 0.14 h_{75}^{-1} \text{ Mpc}$), our deep images show that the central objects are surrounded by extended intra-cluster light elongated in the direction of the distribution of the galaxies described above (cf. Fig. 1, bottom left insert). The size of this intra-cluster light component at the $V = 27 \text{ mag arcsec}^{-2}$ isophote is $\sim 30'' \times 16.7''$, and 2 to 3 times larger at the $V = 31 \text{ mag arcsec}^{-2}$ isophote. There are several very faint clumps in this region surrounded by the diffuse intra-cluster light. The ROSAT X-ray map is too noisy to measure an elongation but its core radius is about $r_{\text{core}} = 37 \pm 6''$ (or $200 \pm 32 h_{75}^{-1} \text{ kpc}$) from Vikhlinin et al. (1998). With redshifts for only 14 galaxies and with a limited spatial coverage it is difficult to estimate the mass of the cluster. We use the standard virial mass estimator (Limber & Mathews 1960; Carlberg et al. 1996), but we complement our estimates with an independent check from the measured X-ray luminosity for this cluster:

$$M_v = \frac{3}{G} \sigma_{1D}^2 r_v,$$

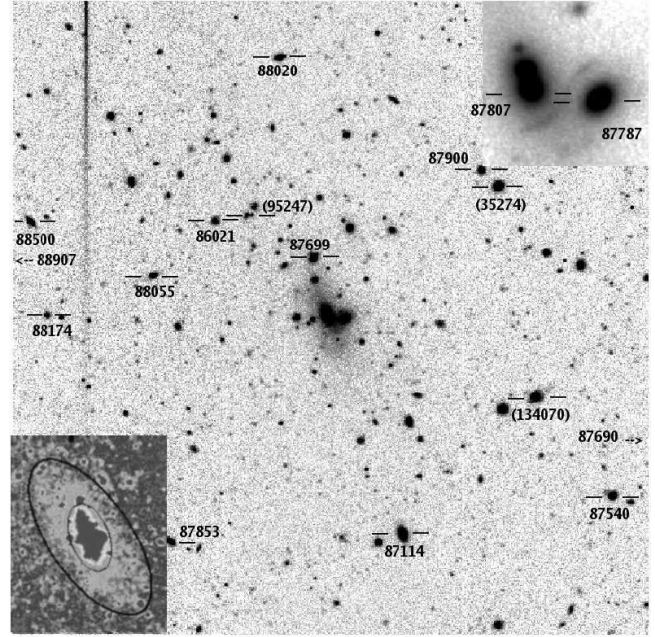


Fig. 1. The V-band image ($4'' \times 4''$) in log intensity scale centered on RX J0054.0-2823. The total exposure time is 7200s, and the seeing $0.8''$ FWHM. The radial velocities are super-imposed to the galaxies (in km sec^{-1}). Velocities of galaxies outside the field are marked by arrow. The velocity 95247 km s^{-1} corresponds to two galaxies. Therefore we have measured the velocity dispersion for 18 objects in the field. The upper insert is the central $16'' \times 16''$ region where the S-shaped feature is visible between the three central galaxies. The lower insert is the $59'' \times 75''$ central region binned 9×9 pixels and it shows the intergalactic light. The inner (outer) ellipse delineates the $V = 27(31) \text{ mag arcsec}^{-2}$ -contour. Both have similar ellipticities $\epsilon = 1 - b/a \sim 0.4$ and orientations, $\theta \sim 20^\circ$ ($\sim 30^\circ$). North is to the top, East is to the left.

where σ_{1D} is the line-of-sight velocity dispersion, and r_v is the virial radius defined as $r_v = \pi R_h / 2$, with R_h the projected harmonic radius

$$R_h = \left\langle \frac{1}{\|\mathbf{R}_i - \mathbf{R}_j\|} \right\rangle_{\text{Pairs}},$$

where \mathbf{R}_i is the projected galaxy position vector. The galaxies used to perform this analysis are chosen to be at a distance equal or lower to 0.25 mag to the red-sequence at redshift $z=0.25$. This selection criteria is illustrated in Fig. 2.

The above estimates are valid only when the distribution of galaxies is spherically symmetric, and in our case we note a considerable elongation in the density distribution. We do only an order or magnitude estimate in this section, pointing out that it has been noticed in the past that spherical dynamic models can reproduce accurately the dynamics of *slightly* elongated systems (Sand, Treu & Ellis 2002; Kronwitter et al. 2000).

The redshift distribution of the 18 objects is shown in Fig. 3: 14 of the 18 measured galaxies are cluster members with velocities around $\sim 88000 \text{ km s}^{-1}$. The remaining four galaxies are a very close pair of faint objects at $\sim 95250 \text{ km s}^{-1}$, a background galaxy at 134070 km s^{-1} and a foreground galaxy at

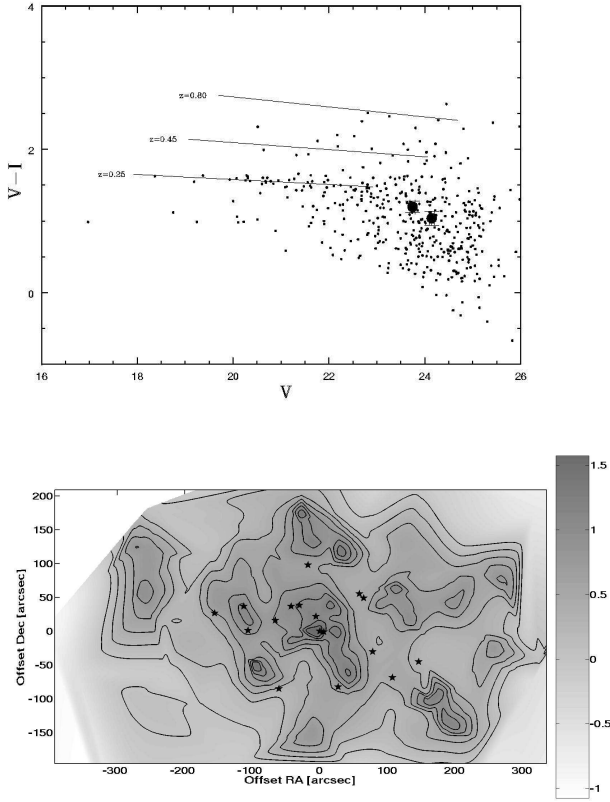


Fig. 2. Top panel: Cluster color-magnitude diagram showing the positions of the red-sequence, the two arcs (big black dots), and the locus of red-sequence expected for redshifts of 0.25, 0.45, and 0.80 according to Kodama et al. (1998). Bottom panel: Contour map of the \log_{10} of galaxy density selecting only galaxies within 0.25 mag from the red-sequence. The stars mark the position of galaxies with measured redshift. The density is in unit of galaxies per square arcminute, and the contour are separated by 0.2 dex intervals. North is to the top, East is to the left.

35275 km s^{-1} (not plotted in the histogram). For the cluster members the distribution is well peaked at $cz=87775 \text{ km s}^{-1}$ with a dispersion $\sigma=675 \text{ km s}^{-1}$. The average coincides with the mean of two of the main central galaxies (#128 and #131), in good agreement with the redshift $z=0.292$ given by Mullis et al. (2003) for the cluster. The internal error in the galaxy redshifts is $\Delta v=209 \pm 30 \text{ km s}^{-1}$, so the intrinsic line-of-sight (rest frame) radial velocity dispersion of the cluster is $\sigma_{1D} = \sqrt{\sigma^2 - \Delta v^2/(1+z)}=497 \text{ km s}^{-1}$, and the 3D dispersion $\sigma_{3D} = \sqrt{3} \sigma_{1D}=860 \text{ km s}^{-1}$. The harmonic radii of the galaxies with velocities and of the galaxies in the red-sequence are $410 h_{75}^{-1} \text{ kpc}^{-1}$ and $710 h_{75}^{-1} \text{ kpc}^{-1}$, respectively. With this value for the velocity dispersion, and with the above values for the harmonic radius we obtain a virial cluster mass in the range $(1 - 2) \times 10^{14} h_{75}^{-1} M_{\odot}$. The luminosity of the galaxies in the red sequence within the corresponding radii are $1.76 \times 10^{11} h_{75}^{-2} L_{\text{Vodot}}$ and $3.06 \times 10^{11} h_{75}^{-2} L_{\text{Vodot}}$. The derived M/L ratios are $570 h_{75} M_{\odot}/L_{\text{Vodot}}$, and $650 h_{75} M_{\odot}/L_{\text{Vodot}}$,

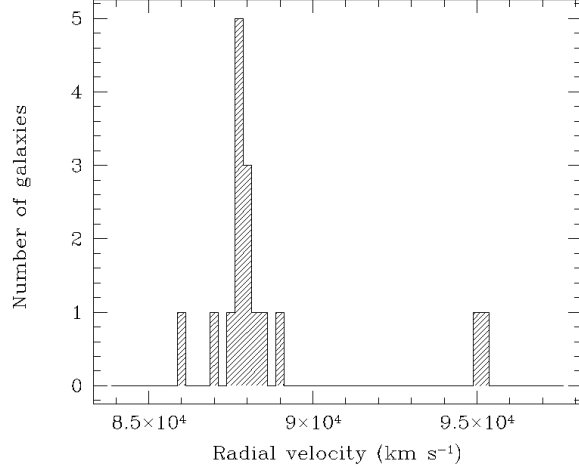


Fig. 3. Velocity histogram of the 16 galaxies in the central region of RX J0054.0-2823 (bin size 250 km s^{-1} ; two galaxies outside range).

respectively. This large M/L values have to be seen as upper limit as they are derived considering only galaxy part of the red-sequence.

The X-ray luminosity of the cluster is $L_X = 0.63 \times 10^{44} h_{75}^{-2} \text{ erg s}^{-1}$ (Vikhlinin et al. 1998). According to Reiprich & Böhringer (2002), with this luminosity and the mass determined above, RX J0054.0-2823 is right in the correlation between X-ray luminosity and cluster virial mass in the region of the least massive clusters.

The approximate linear arrangement of the galaxies, and the clumpy general appearance suggest that the region is probably dynamically young and that the triple central galaxy system could be the merging progenitor of a future single large cD. In addition to the X-ray emitting hot gas, the central potential well appears to be filled with smooth intra-cluster stellar light and the faint sub-galaxian clumps could be material ejected from the interacting system. A composite spectrum in the wavelength range 365 – 420nm was built with the 14 cluster galaxy spectra in order to characterize the presence of star formation following the method of Dressler et al. 2004. This spectrum indicates that there has been no significant star formation in this region for several Gyr (e.g. weak H δ and [OII]).

4. The S-shaped arc

As shown in Fig. 1 (insert top right) and in Fig. 4 (top left panel) there is a giant arc with a total length of $\sim 11''$ and an

unresolved width ($\leq 0.70''$) superimposed on the intra-cluster light. The arc-like feature as a shape of an "S", slightly inclined South-East to North-West. It embraces the South and East part of galaxy #131 and the West and North part of galaxy #128. The bright northern and southern extensions of the arc have a surface brightness of $V \sim 24$ mag arcsec $^{-2}$, while there is a drop in luminosity in the region that links them.

The (V-I)-color of the arc is $\sim 1.1 \pm 0.1$ for the North component and $\sim 1.0 \pm 0.1$ for the fainter South component (see Fig. 2, top panel). There are various possibilities for the physical origin of this S-shape arc. The color of the arc is consistent with being late type gravitationally lensed galaxies at high redshift. But it is also consistent with being cluster member(s) in the faint end of the luminosity function being tidally deformed in an interaction with the central multiple system. In that case, this S-shaped feature could be either tidal debris from the merging of the massive central galaxies, or one or two tidally disrupted cluster members. At $V \sim 24$ mag arcsec $^{-2}$ it would be much brighter than the tidal features found in Virgo (e.g. Mihos et al. 2005), specially if we consider the Tolman dimming which at this redshift should be approximately 1 mag. Thus, although possible we consider the tidal debris origin to be unlikely. A tidally disrupted galaxy interacting with the bright central galaxies is a possibility that cannot be dismissed. A disc galaxy could in principle create a long tidal tail in the interaction with one of these galaxies which could then be distorted by the other. Although this scenario is highly unlikely a priori, we must remember that it was precisely the peculiar geometry of the system that caught our attention in the first place. In what follows we explore the gravitational lens scenario by modelling the arc-shape with the known galaxy and cluster potentials.

4.1. Gravitational lens modelling

In order to model the S-shape arc as one or more gravitationally lensed background galaxies we need to know the gravitational potentials of the putative deflectors. These can be estimated using the structural parameters of the galaxies as given by their photometry and velocity dispersions. The latter have been estimated from the H and K line-profile widths corrected for instrumental broadening by means of the (weak) emission lines. The velocity dispersions turn out to be similar ~ 370 kms $^{-1}$ for the two main galaxies #128 and #131, corresponding to masses $M_{24} = (3.5 - 3.8) \times 10^{11} h_{75}^{-1} M_{\odot}$ and M/L ratios $(M/L)_{24} \approx 22 h_{75}^{-1} (M/L)_{\odot}$, measured at $V=24$ mag arcsec $^{-2}$. No spectra were taken for galaxy #139, hence no velocity dispersion is measured.

We want to test whether the S-shaped arc can be the distorted, potentially multiple, image of one or more background galaxies. Our simplified lens potential consists of four components at $z = 0.292$: the cluster, and the three central galaxies: #128, #131 and #139 (see Fig. 4). These components are fitted by Pseudo-Isothermal Mass Distributions (PIEMD; Kassiola & Kovner 1993, Kneib et al. 1996) defined by position, core radius, cut radius, orientation, ellipticity, and velocity dispersion. Since the source redshift is not known, we

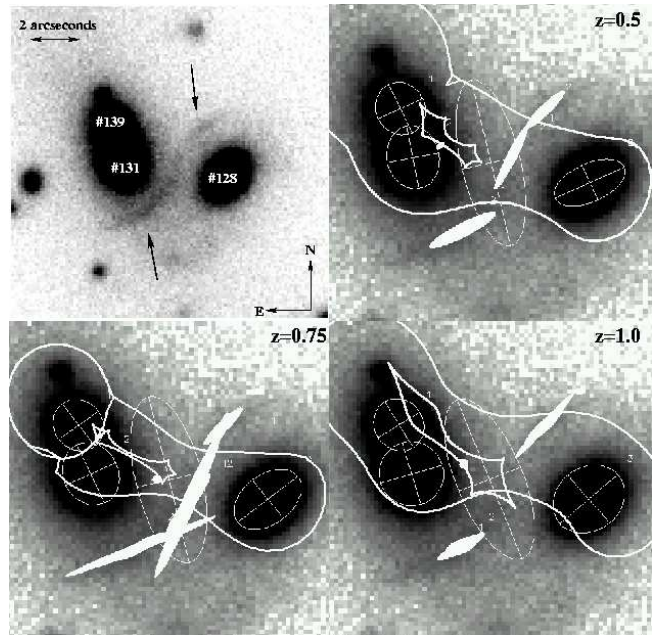


Fig. 4. Top left panel: The S-shape feature in the $10'' \times 10''$ V-band image of the center of RX J0054.0-2823. The names of the galaxies are labeled as in the text and in Table 1. The arrows point at the bright regions of the arc. Top right panel and bottom panels: the lens model for three different source redshifts (indicated in the upper-right corner of each image) superimposed on the central $6'' \times 6''$ V-band image. North is to the top, East is to the left. The ellipsoids filled in white show the location of the images (the source position is represented by a white dot) for the best lens mass model. The white ellipsoids indicate the location, ellipticity, and orientation of the lensing galaxies (#128, #131 and #139) and of the galaxy cluster as given in Table 1. For the galaxy cluster the size is reduced to optimize its visibility in the figure. The white bold solid lines indicates the inner and outer caustic lines for the best lens mass model.

have computed models for four different source redshifts: $z_s = 0.5, 0.75, 1.0$ and 2.0 .

Since the arc has two bright regions (see Figs. 4, top left panel), we initially assumed that it is built by the gravitationally distorted images of two background objects. With these assumptions we used the LensTool package (Kneib et al. 1993) to model the arc in an iterative way varying the input parameters within the ranges allowed by the observations. For the cluster potential the only initial constraint was the velocity dispersion, but since the models are relatively insensitive (within reasonable values) to the cluster center position, we chose to keep it fixed at a value close to the centroid of the three main galaxies (cf. Fig. 4 and Table 1). We iterated until we found solutions that satisfied the following criteria: (a) input parameters consistent with observations; (b) lensed images match the morphology of S-arc. The code naturally converges to a single source for the two arc components, therefore we supposed that the arc is formed by the distorted

Table 1. Parameters of the gravitational lens model: Column 1: Redshift of the source. Column 2: Lens component. Column 3 and 4: Lens position relative to the brightest part of the northern arc component. Column 5: Lens ellipticity. Column 6: Lens position angle. Column 7: Lens velocity dispersion.

Source	Lens	$\Delta x (")$	$\Delta y (")$	ϵ	$\theta (^\circ)$	σ_v (km s ⁻¹)
$z_s=0.5$	#128	-0.81	-1.37	0.49	-65	350
	#131	2.43	-0.89	0.20	11	401
	#139	2.66	0.02	0.10	30	252
	Cluster	1.0	-1.0	0.66	13	940
$z_s=0.75$	#128	-0.81	-1.37	0.34	-51	354
	#131	2.43	-0.89	0.16	36	360
	#139	2.66	0.02	0.10	25	217
	Cluster	1.0	-1.0	0.62	13	811
$z_s=1.0$	#128	-0.81	-1.37	0.10	-43	230
	#131	2.43	-0.89	0.02	30	150
	#139	2.66	0.02	0.10	34	285
	Cluster	1.0	-1.0	0.51	28	618

images of a single background source.

For the fit of the best lens potential, we allow the 3D-velocity dispersion to vary in a 20% error-bar range around the value 870 km s⁻¹ for the galaxy cluster and 370 km s⁻¹ for galaxies #128 and #131. Galaxy #139 being fainter than the two other galaxies of the model, we assume that its mass is lower and put an upper limit on its velocity dispersion of 300 km s⁻¹.

4.2. Results

Our best-fit models for a gravitational lensing scenario are shown in Fig. 4 for three values of the source redshift ($z_s = 0.5, 0.75, 1.0$). A large sample of good fit can be found for the observed parameter error-bars. This illustrates the robustness of the gravitational lensing hypothesis and the high probability of having such a S-shaped arc formed in the heart of such mass potential configuration.

The parameters of our best-fitting models are tabulated in Table 1: for each source redshift we report the position relative to the center of the North bright component of the arc (Δx , Δy), the ellipticity (defined as $\epsilon=1-b/a$, where a is the semi-major axis and b is the semi-minor axis), the position angle (θ , positive North to East counter-clockwise) and the velocity dispersion (σ_v) of the lens components are given.

Our best fits are obtained for source redshifts $0.5 \leq z_s < 1.0$. For $z=1$, we match the galaxy and cluster PA and ellipticity only for velocity dispersions much lower than the measured one (see Table 1). Moreover, we were not able to obtain good fits for $z_s \geq 1$. In fact, the model parameters of the lens components depart increasingly from the observations as the source redshift increases.

According to model for source redshift a $z_s=0.5$ and 0.75 , the arc would be built by 3 images of a single background galaxy: two images in opposite orientation (mirror images) would built the northern part of the arc, one single image would be the southern part. The luminosity drop observed in the northern part of the arc would reflect a decreasing surface bright-

ness region in the galaxy source, that would also be, in the lens plane, the location where the two northern images are partially overlap.

We conclude that gravitational lensing is a natural and very likely explanation for the S-shaped arc observed in RX J0054.0-2823.

5. Summary and conclusion

We report the discovery of an S-shaped arc in the very center of the galaxy cluster RX J0054.0-2823. We discuss various possibilities for the physical origin of the feature. Modelling the potential formed by three massive central galaxies plus the cluster itself, we obtained very good fits to location and shape of this arc for a gravitationally lensed galaxy source at $0.5 \leq z_s < 1.0$. These models show that the S-shaped feature is likely to be the triple gravitational image of a single background galaxy. There is not a unique satisfying solution for the modelling. This implies that lensing is a very natural explanation for the S-arc feature for the configuration observed for the galaxies and the galaxy cluster.

All the best-fitting potential of the cluster have an ellipticity and orientation consistent with the distribution of both the diffuse intra-cluster light, and of the X-ray emission. This, together with the elongated galaxy distribution, and the relatively large mass inferred from the Virial theorem, suggests that the cluster is dynamically young, and probably the result of a recent merging.

Given the success of the lensing modelling, the alternative explanations of tidally induced compression of the stellar intra-cluster medium, or a highly distorted cluster spiral appear rather unlikely. The gravitational lensing explanation only works if the redshift of the source is lower than $z_s \sim 1$. Therefore, a straightforward test for the lensing hypothesis is to measure the redshift of the arc.

Acknowledgements. C.F. and J.W. are supported by the European Community's Sixth Framework Marie Curie Research Training Network Programme, Contract No. MRTN-CT-2004-505183 "ANGLES" and granted by the ECOS-CONYICIT Committee. H.Q. is grateful for partial support from the FONDAP Astrophysics Center.

References

- Bartelmann M., Huss A., Colberg J.M., Jenkins A. & Pearce F.R., 1998, A&A 330, 1
- Carlberg R. G., Yee H. K. C., Ellingson E., Abraham R., Gravel P., Morris S. & Pritchet C.J., 1996, ApJ 462, 32
- Colley W. N., Tyson J.A. & Turner E.L. 1996, ApJ 461, L83
- Dressler A., Oemler A.J., Poggianti B.M., Smail I., Trager S., Shectman S.A., Couch W.J. & Ellis R.S., 2004, ApJ 617, 867
- Gladders M.D., Yee H.K.C. & Ellingson E., 2002, AJ 123, 1
- Golse G., Kneib J.-P. & Soucail G. 2002, A&A 387, 788
- Kassiola A. & Kovner I. 1993, ApJ 417, 450
- Kneib J.-P., Mellier Y., Fort B. & Mathez G., 1993, A&A, 273, 367
- Kneib J.-P., Ellis R.S., Smail I., Couch W.J. & Sharples R.M., 1996, ApJ 471, 643

- Kronawitter A., Saglia R.P., Gerhard O. & Bender R., 2000, A&AS144, 53
- Kodama T., Arimoto N., Barger A. & Aragón-Salamanca A., 1998, A&A334, 99
- Landolt A.U., 1992, AJ, 104, 340
- Limber D. N. & Mathews W. G., 1960, ApJ132, 286
- Lynds R. & Petrosian V., 1986, Bull. AAS, 18, 1014
- Melnick J., Selman F. & Quintana H., 1999, PASP 111, 1444
- Mihos J.C., Harding P., Feldmeier J. & Morrison H., 2005 ApJ, 631, 41
- Mullis C.R., McNamara B.R., Quintana H., Vikhlinin A., Henry J.P., Gioia I.M., Hornstrup A., Forman W. & Jones C., 2003, ApJ 594, 154
- Paczyński B., 1987, Nature 325, 572
- Reiprich T. & Böhringer H., 2002 ApJ567, 716
- Sand D.J., Treu T. & Ellis R. S., 2002 ApJ, L129
- Sand D.J., Treu T., Ellis R.S. & Smith G.P., 2005, ApJ 627,32
- Soucail G., Fort B., Mellier Y., & Picat J.-P., 1987, A& A 172, L14
- Soucail G., Kneib J.-P. & Golse G., 2004, A&A417, L33
- Vikhlinin A., McNamara B.R., Forman W., Jones C., Quintana H. & Hornstrup A., 1998, ApJ 502, 558
- Wambsganss J., Bode P. & Ostriker J.P., 2004, ApJ 606, L93
- Wambsganss J., Schneider P., Giraud E., Weiss A., 1989, ApJ 337, L73